nature physics

Perspective

https://doi.org/10.1038/s41567-024-02656-0

Thirty years of puzzling superconductivity in Sr_2RuO_4

Received: 29 January 2024

Accepted: 30 August 2024

Published online: 11 November 2024

Check for updates

Y. Maeno ✉, A. Ikeda & G. Mattoni

Superconductivity in Sr_2RuO_4 was discovered 30 years ago. Among the many intriguing aspects of this unconventional superconductor is the picture of spin-triplet superconductivity, which could potentially carry both charge and spin supercurrents. This proposal was considered for a long time but was ultimately disproven in 2019. Despite intense research over the past several years, the superconducting symmetry of the archetypal unconventional superconductor Sr_2RuO_4 remains unresolved. Here we highlight the recent controversies and give a perspective of how the final resolution may be reached.

Superconductivity in the layered oxide Sr_2RuO_4, which is isostructural to the first-discovered copper oxide high-temperature superconductor[1], was first reported in 1994[2]. Its superconducting transition temperature T_c is strongly dependent on sample quality, and it is 1.5 K in the best crystals. Because of its unconventional superconductivity, evidenced by its extreme sensitivity to non-magnetic impurities[3], and the strong electron correlations observed in the Mott insulating sister compound Ca_2RuO_4 (ref. 4), Sr_2RuO_4 is considered an archetypal quantum material. Despite extensive research efforts and state-of-the-art experimental and theoretical studies, understanding its puzzling superconducting state remains a challenge[5]. In Box 1, we introduce some key terms used to describe the peculiar features of unconventional superconductivity.

The electronic state of Sr_2RuO_4 contains typical complications of quantum materials exhibiting emergent properties, such as exotic superconductivity and magnetism. It features strong electron correlations, moderate spin–orbit coupling and a superconducting state that involves more than one electronic orbital. The normal state of Sr_2RuO_4 exhibits textbook-like Fermi-liquid properties at low temperatures[6], in stark contrast to the exotic normal-state properties of other well-known unconventional superconductors, such as copper oxide, iron-based and heavy fermion superconductors. Its highly correlated, quasi-two-dimensional (2D) electronic structure has been accurately characterized by angle-resolved photoemission spectroscopy and quantitatively understood down to fine details by electronic structure calculations[7]. Importantly, chemically stable, extremely high-quality single crystals have been grown by several groups using the floating-zone method (Fig. 1), and experimental results from different research groups are highly reproducible as long as the same type of probe is used. Therefore, we believe that complete understanding of the basic superconducting properties of Sr_2RuO_4 is possible.

Controversies about the superconducting symmetry

Over the past 30 years, Sr_2RuO_4 has challenged key experimental techniques. The angle-resolved photoemission spectroscopy measurements reported by two expert groups were initially believed to be associated with bulk properties. However, years later, an essential revision was made because of the presence of surface states caused by the rotation of the RuO_6 octahedra on the cleaved surface[8]. For this reason, the Γ band, which hosts a van Hove singularity, was initially reported as a hole band, rather than as an electron band.

In 2019, another key result concerning the spin state of the superconducting electrons was found to be incorrect[9]. Owing to the extremely high in-plane conductivity of Sr_2RuO_4, eddy-current joule heating by radio-frequency pulses during nuclear magnetic resonance (NMR) measurements increased the sample temperature above T_c. Even if such overheating lasted up to only 10 ms, it was enough to alter the results[10]. For this reason, the NMR pulse energy for Sr_2RuO_4 needs to be reduced to an unusually low level to observe the correct shift of the resonance line—the Knight shift—associated with the reduction of spin susceptibility in the superconducting state. This precaution may also apply to other low-T_c superconductors, especially those with extremely low residual resistivity. These findings have encouraged NMR researchers to present their results as a function of pulse energy, thereby demonstrating that overheating does not occur during the measurement process.

With additional NMR results under different in-plane field directions, it was concluded that the Cooper-pair spin state is singlet and thus not compatible with either chiral or helical spin-triplet states[11]. Another experiment involving polarized neutrons that previously concluded in favour of triplet pairing was repeated under lower applied

Toyota Riken – Kyoto University Research Center (TRiKUC), Kyoto University Institute for Advanced Study, Kyoto, Japan.
✉e-mail: maeno.yoshiteru.b04@kyoto-u.jp

https://doi.org/10.1038/s41567-024-02656-0

BOX 1

Unconventional superconductivity

Superconductivity is usually called 'conventional' when it is described by the original Bardeen–Cooper–Schrieffer (BCS) theory[48], which involves spin-singlet *s*-wave pairing. Superconducting states not described by the BCS theory are usually referred to as 'unconventional' and involve other types of pairing.

The fermionic nature of electrons gives rise to antisymmetric states, meaning that the state vector undergoes a minus sign change upon particle exchange. An antisymmetric spin-singlet state can be represented as $\frac{1}{\sqrt{2}}\{|\uparrow\downarrow\rangle - |\downarrow\uparrow\rangle\}$ (in which ↑ and ↓ represent spin-up and spin-down states, respectively), and it must be accompanied by an orbital wavefunction of even parity that corresponds to orbital angular momentum, such as $L=0$ (*s* wave), $L=2$ (*d* wave) and $L=4$ (*g* wave). Conversely, the spin-triplet states of the form $|\uparrow\uparrow\rangle$, $|\downarrow\downarrow\rangle$ or $\frac{1}{\sqrt{2}}\{|\uparrow\downarrow\rangle + |\downarrow\uparrow\rangle\}$ must be accompanied by odd-parity orbital states, such as $L=1$ (*p* wave) and $L=3$ (*f* wave). High-temperature copper oxide superconductors, many of the heavy-electron superconductors and organic superconductors are believed to be in spin-singlet *d*-wave states. Naively, strong electron correlations with strong Coulomb repulsion in these unconventional superconductors disfavour *s*-wave pairing, where the maximum amplitude of the order parameter is achieved when the paired electrons are at zero distance between each other. However, such a simple classification may partially break down if the spin–orbit coupling is strong. Among the unconventional superconductors, there are some promising candidates for spin-triplet pairing, but a complete characterization of these superconducting states has not been achieved so far. The superconducting energy gap of unconventional superconductors is often accompanied by the presence of nodes in the momentum space around which the order-parameter phase changes its sign.

Among unconventional superconductors, some exhibit exotic properties, including the breaking of time-reversal symmetry (TRS) and rotational symmetry. TRS is the property under which a physical system is unchanged upon reversal of time, whereas rotational symmetry is the property under which a physical system remains unchanged upon rotation of a certain angle. Systems showing broken TRS for intrinsic reasons are often called 'chiral' or 'non-unitary', depending on whether the symmetry breaking originates from the orbital or spin part of the order parameter. Systems where the rotational symmetry of the electronic structure is spontaneously broken in the superconducting state are often called 'nematic'. According to the irreducible representation to which it belongs, the superconducting order parameter can be classified as 1D if it is described by a single function or 2D if it is described by a pair of functions. Chiral TRS breaking can be realized using a 2D order parameter. Topological superconductors have an order parameter characterized by a topological invariant, a quantity that does not change upon deformation of the space, and have specific edge states at the boundary based on bulk–edge correspondence. Spin-singlet and triplet superconducting states with chiral TRS breaking have topological properties.

field, and it manifested the reduction of the magnetic susceptibility as expected for a singlet pairing[12]. Thus, the superconducting symmetry of Sr_2RuO_4 took a turn from 'spin-triplet chiral *p*-wave pairing' to 'spin-singlet pairing'.

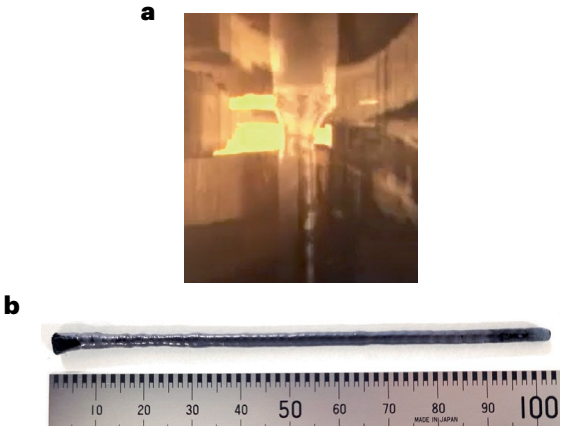

Fig. 1 | Crystal growth of Sr_2RuO_4 using the floating-zone method. a, Large, high-quality single crystals of Sr_2RuO_4 that exhibited $T_c = 1.50$ K were grown using the floating-zone method. A feed rod (diameter of 6 mm) of sintered powder was used, and the (001) facet parallel to the RuO_2 plane was clearly visible. **b**, Typical crystal with a cross-section of 3×4 mm^2 and length of up to 100 mm (ref. 46).

This development forced us to re-examine other existing results from a new viewpoint. Nevertheless, the symmetry of the superconducting state of Sr_2RuO_4 has not yet been unanimously agreed on at present. Meanwhile, a serious controversy among the key results has become evident. Two main issues that currently prevent us from reaching a consensus among the candidate superconducting states are illustrated in Fig. 2: (1) whether the TRS is broken or not and (2) whether there is a horizontal line node in the superconducting gap in addition to the vertical line nodes or gap minima. For the examples shown in Fig. 2, the latter issue also corresponds to whether the order parameter dimensionality is one-dimensional (1D) or 2D. We examine these issues in the following sections.

Does the superconductivity of Sr_2RuO_4 break TRS?

Of equal importance to the NMR result, another key experimental result is the TRS breaking of the order parameter, which is based on the observation of the spontaneous internal magnetic field emerging below T_c in a muon spin rotation (μSR) experiment[13]. The internal magnetic field detected at the muon site has been interpreted to be a consequence of the topological edge current around either impurities or the implanted muon itself in a TRS broken superconductor. The observation of TRS breaking signals in Sr_2RuO_4 is robust and reproducible among different investigators and muon facilities[14–17]. The broken TRS state was also detected using the magneto-optic Kerr effect[18]. Recently, ab initio theories for the normal state of Sr_2RuO_4 have been used to identify the muon stopping site and determine the influence of a muon in the electronic states[19,20]. The positive charge of an injected muon with its lifetime of 2.2 μs substantially distorts the lattice, but because of the short Thomas–Fermi screening length of about 0.1 nm, the effect is rather local. In the superconducting state, the charge screening length is expected to be essentially unchanged[21].

The innovative development of a uniaxial-stress apparatus using piezo stacks introduced new insights into the study of Sr_2RuO_4 (ref. 22). Uniaxial stress along the [100] direction enhanced T_c from 1.5 to 3.5 K (ref. 23), thus answering the long-standing question of the mechanism of T_c enhancement in the eutectic '3-K phase'[24]. Uniaxial stress, which breaks the tetragonal symmetry of the lattice, provides important information concerning the TRS breaking. The superconducting onset T_c increases with uniaxial stress, whereas the temperature at which muons start to experience an emerging magnetic field T_{TRSB} remains almost the same or decreases slightly[16]. As the splitting between T_c and T_{TRSB} was observed only when the tetragonal crystalline symmetry was

https://doi.org/10.1038/s41567-024-02656-0

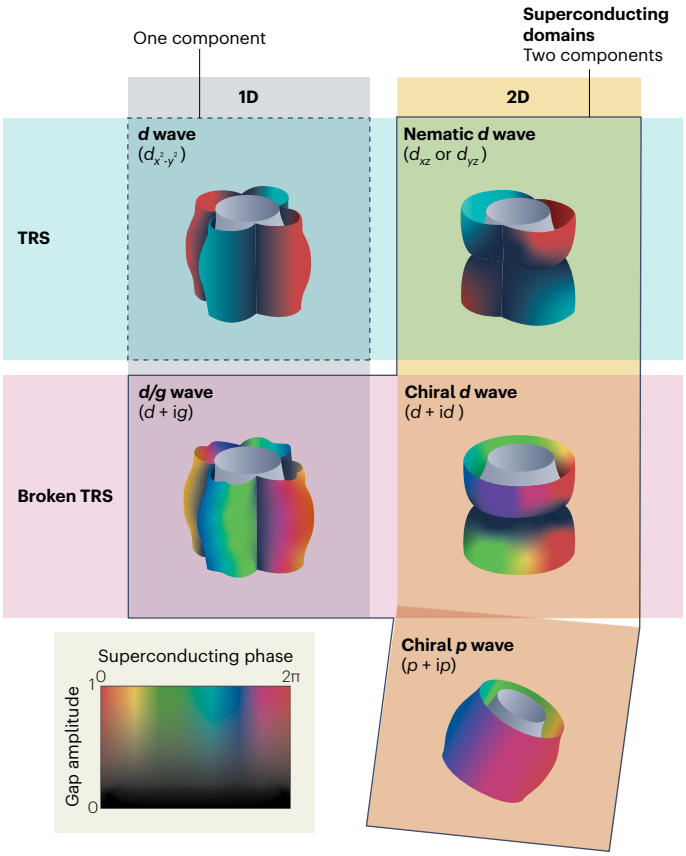

Fig. 2 | Some of the proposed superconducting symmetries of Sr_2RuO_4. To identify the superconducting state of Sr_2RuO_4, some controversies among the observed results need to be resolved. Left, 1D irreducible representation states: *d*-wave (top) and accidentally degenerate *d* + i*g*-wave (bottom) states. Right, 2D irreducible-representation states: nematic *d*-wave (top) and chiral *d* + i*d*-wave (middle) states. Previously proposed spin-triplet, chiral *p*-wave state (bottom right) is not consistent with the recent NMR results. The time-reversal symmetry (TRS) is preserved for only the top two states; superconducting domains under the tetragonal crystal symmetry may form in the three states, except for the *d*-wave state on the top left[5,47]. The colours depict the superconducting gap amplitude and phase as shown on the bottom left. Diagrams reproduced with permission from: TRS and broken TRS rows, ref. 5, Physical Society of Japan; chiral *p* wave, ref. 47, Association of Asia Pacific Physical Societies.

broken, it was suggested that the degeneracy between T_c and T_{TRSB} was symmetry protected[17].

The μSR results, however, have recently been challenged by thermodynamic measurements searching for the second transition at T_{TRSB}. The heat capacity C_P indicates a clear jump in C_P/T at T_c as it increased to 3.5 K under [100] strain[25]. However, there was no sign of any additional jump anticipated at T_{TRSB} (ref. 24). Furthermore, elastocaloric measurements did not probe any sign of the anticipated second transition[26]. A possible explanation is that the entropy release at the second transition is small or broadened in the thermal measurements[27]. An increasing number of superconductors seem to demonstrate a signature of broken TRS in μSR measurements[28], including some with simple *s*-wave character, raising some doubts about whether all μSR data are being correctly interpreted as detections of TRS breaking. Another possibility for Sr_2RuO_4 is that the presence of surface magnetism in the normal state, observed with ultraslow muons[29], may lead to spontaneous vortices in the bulk below T_c.

As a related development on the multicomponent order parameter, two groups have recently reported an unusual jump in a c_{66} shear-mode ultrasound velocity at T_c, in addition to the ordinary jumps in the compressional modes[30,31]. This implies that the superconducting order parameter is in specific irreducible representations: E_g, $B_{1g}\oplus A_{2g}$ or $B_{2g}\oplus A_{1g}$. Considering this requirement and depending on whether the TRS is considered broken, the two groups proposed different superconducting order parameters: nematic E_g state with the gap structure d_{xz} or d_{yz} that does not break TRS and accidental TRS breaking $B_{1g}\oplus A_{2g}$ with the gap $d + ig$.

As shown in Fig. 2, for 2D (E_g) and two-component 1D order parameters, a superconducting domain structure may form in the crystallographic single-domain material: $d_{xz} + id_{yz}$ and $d_{xz} - id_{yz}$ domains for TRS breaking chiral superconductors and d_{xz} and d_{yz} for nematic superconductors. Various phenomena observed only in undistorted Sr_2RuO_4 are attributed to the phase interference between such coexisting domains[32].

Horizontal line node and interorbital pairing

Determination of the superconducting gap anisotropy, especially the characterization of the location of the gap nodes, is essential for identifying the superconducting symmetry and mechanisms. The temperature and field dependence of the specific heat suggests the presence of line nodes or strongly suppressed gaps. The location of the node in the superconducting gap was investigated using the specific heat under a magnetic field applied in various directions[33,34]. The experimental data of the two groups were consistent with each other. If interpreted in terms of vertical line nodes or vertical gap minima, the nodal direction is along the Γ–M direction[33]. This interpretation is consistent with either $p + ip$ or d_{xy} symmetry but inconsistent with $d_{x^2-y^2}$ symmetry. Extending the measurements down to temperatures as low as 0.04 T_c, Kittaka et al. did not observe the anticipated reversal of the oscillatory phase of the four-fold specific heat oscillations with respect to the in-plane field direction[34]. These results led the authors to conclude that there was a horizontal line node in the superconducting order parameter. In this case, the origin of the oscillation in the specific heat is the four-fold anisotropy of the quasiparticle Fermi velocity around the horizontal line node. Thermal conductivity measurements

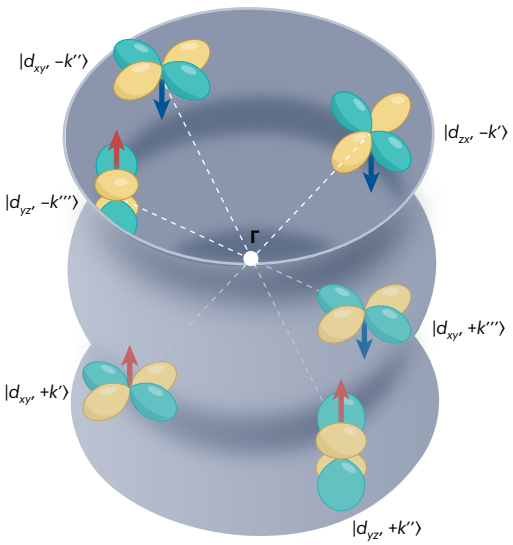

Fig. 3 | Interorbital pairing state proposed for Sr_2RuO_4. In the orbital basis, a Cooper pair on the same band in the reciprocal space consists of electrons of the orbitals d_{xy} and either d_{yz} or d_{zx} with opposite momenta k' (k'', k''') and $-k'$ ($-k''$, $-k'''$), forming a spin-triplet ($|\uparrow\downarrow\rangle + |\downarrow\uparrow\rangle$), orbital-antisymmetric, even parity state. When transformed into the band basis, it is a spin-singlet, *d*-wave state with a symmetry-protected horizontal line node and gap minima along the vertical direction. Although rather exotic, such a state can explain many of the observed facts. The different colours of the orbital wave-function envelopes represent different phases.

https://doi.org/10.1038/s41567-024-02656-0

BOX 2

Bridging pressure and ultrasound experiments

Here we discuss how available results obtained from different techniques can be compared, leading to the two controversies introduced in the main text regarding the kink and slope of the variations in T_c with strain. On the one hand, Hicks et al. applied uniaxial pressure reporting that the change in T_c with respect to the strain ε induced by the stress σ in the [110] direction is smooth and does not exhibit any kink at $\varepsilon_{<110>}=0$ (ref. 22). As illustrated in panel **a**, $\varepsilon_{<110>}$ can be decomposed into two components: a volume-conserving shear strain ε_6 (also written as ε_{12} or ε_{xy}) and an in-plane compression $\varepsilon_{A1g,1}=\varepsilon_1+\varepsilon_2$ (also written as $\varepsilon_{11}+\varepsilon_{22}$ or $\varepsilon_{xx}+\varepsilon_{yy}$). For the first component, we note that the effect of a positive ε_6 is equivalent to a negative ε_6 because of the four-fold rotational symmetry of the lattice. Therefore, if T_c changes with a positive ε_6, it should also change by the same amount with a negative ε_6, or $\Delta T_c \propto |\varepsilon_6|$, leading to a kink in T_c versus $\varepsilon_{<110>}$ at $\varepsilon_{<110>}=0$. For the second component, $\varepsilon_{A1g,1}$ does not lead to a kink because positive and negative $\varepsilon_{A1g,1}$ should result in changes in ΔT_c of the opposite sign. Thus, the experimental absence of a kink in T_c versus $\varepsilon_{<110>}$ indicates that T_c is insensitive to ε_6. On the other hand, ultrasound experiments revealed a jump in c_{66} across T_c (refs. 30,31). The ultrasound results, in combination with the Ehrenfest relation described below, indicate that T_c depends on ε_6, contradicting the uniaxial pressure result. A detailed quantitative analysis of this controversy was conducted by Jerzembeck et al.[49].

As a second issue, we examined the initial slope of the T_c variations with strains. The change in T_c with uniaxial stress in the *c*-direction σ_3 (also written as σ_{33} or σ_{zz}) was reported as $\partial T_c/\partial\sigma_3=+76\,\mathrm{mK\,GPa^{-1}}$ (ref. 41). In addition, the change in T_c with hydrostatic pressure P_{hyd} was reported as $dT_c/dP_{hyd}\approx-0.21\,\mathrm{K\,GPa^{-1}}$ (ref. 42). We note that P has the opposite sign to both σ and ε; positive P corresponds to lattice compression, whereas positive σ and ε correspond to lattice expansion. As the hydrostatic pressure is a combination of the in-plane compression $\sigma_{A1g,1}=(\sigma_1+\sigma_2)/2$ (also written as $(\sigma_{11}+\sigma_{22})/2$ or $(\sigma_{xx}+\sigma_{yy})/2$) and the *c*-axis compression σ_3 as illustrated in panel **b**, we calculated from the experimental results

$$\frac{\partial T_c}{\partial \sigma_{A1g,1}} = -\frac{dT_c}{dP_{hyd}} - \frac{\partial T_c}{\partial \sigma_3} \approx 0.13\ \mathrm{KGPa^{-1}}.$$

As shown in panels **c** and **d**, we used this expression along with elastic moduli c_{11}, c_{12}, c_{13} and c_{33} (reported in ref. 31) to calculate the strain dependence of T_c, as shown in the left column of the table below. These results are compared with the changes in T_c predicted by compressional ultrasound in the right column of the table below, in which the initial slope $\partial T_c/\partial\sigma_i$ (i represents $A_{1g,1}$ or 3) is linked to the jump of the elastic modulus c_i by the thermodynamic Ehrenfest relation[30,31,50,51], with ΔC_P the jump at T_c of the specific heat per volume. We note that there is a prefactor on the left-hand side of this equation depending on mode i and the coefficients in the Ginzburg–Landau free energy, which, for the cases discussed here, is equal to unity[51]. Using the values $T_c=1.42$ K, $\Delta C_P=33\,\mathrm{mJ\,mol^{-1}K^{-1}}=570\,\mathrm{J\,m^{-3}K^{-1}}$ and Δc_i from ref. 31, we can estimate the strain dependence of T_c again. These values obtained from ultrasound in the right column are about a factor of 5 larger than those calculated using the pressure experiments in the left column.

As an additional final comparison, we note that the jump in c_{11} in the pulse–echo ultrasound experiment[30] implies $|\partial T_c/\partial\varepsilon_1|=1.08\,\mathrm{K\%^{-1}}$ from the Ehrenfest relation combined with the fact that little jump is observed in the shear mode $(c_{11}-c_{12})/2$.

This large variation in T_c is in sharp contrast to the absence of an initial slope under [100] uniaxial stress[22,23,44].

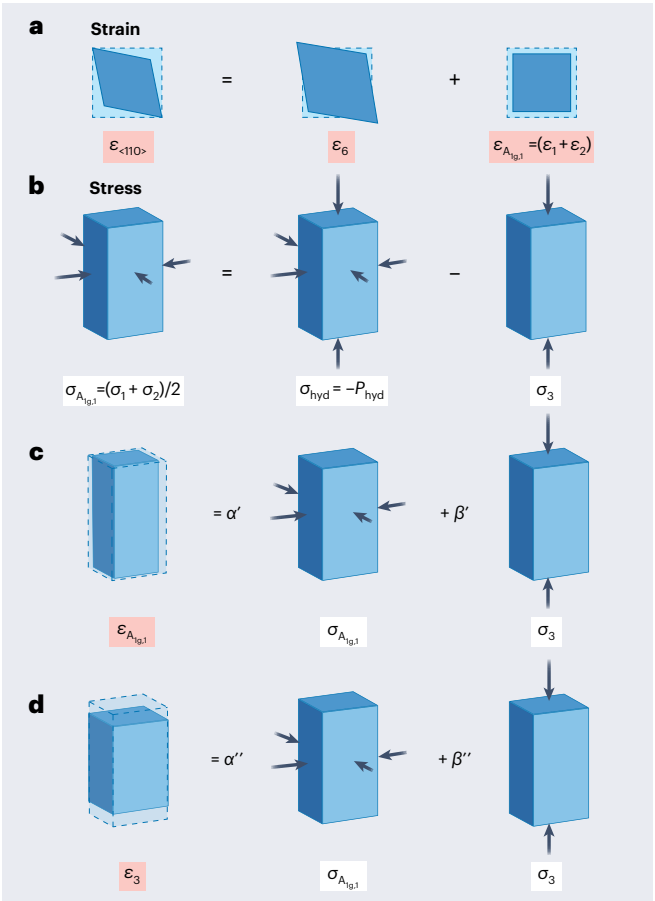

Relationships between strain and stress. a, Uniaxial strain in the [110] direction can be described as the sum of a volume-preserving shear deformation and a biaxial strain. **b**, In-plane biaxial stress can be described as the hydrostatic pressure minus the out-of-plane stress. **c**,**d**, Biaxial strain (**c**) and out-of-plane strain (**d**) can be described as combinations of stresses with different coefficients α and β.

Changes in T_c by strain calculated from the pressure experiments via the elasticity tensor (left) and compressional ultrasound experiments via the Ehrenfest relation (right)

Pressure experiments	Sound velocity
$\frac{\partial T_c}{\partial \varepsilon_i} = \sum_j \frac{\partial \sigma_j}{\partial \varepsilon_i}\frac{\partial T_c}{\partial \sigma_j} = \sum_j c_{ji}\frac{\partial T_c}{\partial \sigma_j}$	$\left(\frac{\partial T_c}{\partial \varepsilon_i}\right)^2 = \frac{-T_c\Delta c_i}{\Delta C_P}$: Ehrenfest relation
$\frac{\partial T_c}{\partial \varepsilon_{A1g,1}} = \frac{c_{11}+c_{12}}{2}\frac{\partial T_c}{\partial \sigma_{A1g,1}} + c_{13}\frac{\partial T_c}{\partial \sigma_3} \approx 0.32\,\mathrm{K\%^{-1}}$	$\left\lvert\frac{\partial T_c}{\partial \varepsilon_{A1g,1}}\right\rvert = \sqrt{\frac{-T_c\Delta c_{A1g,1}}{\Delta C_P}} = 1.59\,\mathrm{K\%^{-1}}$
(panel **c**)	
$\frac{\partial T_c}{\partial \varepsilon_3} = c_{13}\frac{\partial T_c}{\partial \sigma_{A1g,1}} + c_{33}\frac{\partial T_c}{\partial \sigma_3} \approx 0.31\,\mathrm{K\%^{-1}}$	$\left\lvert\frac{\partial T_c}{\partial \varepsilon_3}\right\rvert = \sqrt{\frac{-T_c\Delta c_3}{\Delta C_P}} = 1.56\,\mathrm{K\%^{-1}}$
(panel **d**)	

under a rotating in-plane magnetic field also concluded in favour of a horizontal line node[35].

Several experiments have been conducted to probe the low-energy quasiparticle excitations in this system. Thermal conductivity measurements indicate that low-energy quasiparticles have a Fermi velocity component along the *c* axis[36]. Measurements of the penetration depth by μSR[37], scanning-probe superconducting interference devices[38] and a.c. susceptibility[39] suggest line nodes along the interlayer *c* direction (vertical line nodes). It should be noted that gap models with only vertical line nodes are often compared with models with only a horizontal line node[5]. These analyses conclude the presence of vertical line nodes but do not necessarily exclude the presence of an additional horizontal line node.

The horizontal line node, if it is at the interlayer wave number $k_z = 0$, is not natural for quasi-2D materials, such as Sr_2RuO_4, because it implies that intralayer pairing is not allowed. An interorbital pairing model was proposed as a microscopic mechanism that allows a horizontal line node[40]. It first examines the pairing in the orbital basis and then transforms it into the band basis using a realistic three-dimensional orbital-characterized three-band electronic structure. As a promising candidate, a spin-triplet $(|\uparrow\downarrow\rangle + |\downarrow\uparrow\rangle)$, *s*-wave, orbital-antisymmetric (orbital-singlet) pairing state has been proposed. This state is depicted in Fig. 3. This state belongs to the 2D irreducible representation E_g and transforms into a spin-singlet, *d*-wave superconducting state on the band basis. It has an approximate vertical line node in addition to the horizontal line node in the gap, and the TRS can be either broken (chiral) or not (nematic). These interorbital E_g states have some similarities to the traditional intra-orbital E_g states shown in Fig. 2. The order parameters with E_g symmetry must change sign by reflection on the x–y plane and lead to a horizontal line node at $k_z = 0$. The interorbital model further explains its origin on a microscopic basis. In essence, if the pairing is between electrons with d_{yz} (d_{xz}) and d_{xy} orbitals, the symmetry information encoded in the first orbital captures the sign change by x–y-mirror reflection[5]. Whether such an exotic pairing state can be realized remains an open question to be resolved by further experimental investigation. However, the interorbital pairing model can explain the following unusual observations under strains[5,27]: T_c decreases under uniaxial strain along the *c* axis[41], despite the increase in the electronic density of states; T_c decreases under hydrostatic pressure[42], under which the Fermi surface becomes more 2D, thus weakening the interlayer coupling. Furthermore, a theory predicts an anisotropic reduction of the Knight shift in such a spin-triplet interorbital pairing, distinct from the spin-singlet pairing[43].

Controversies among various lattice-distortion experiments

As described previously, the application of uniaxial strains has provided some fresh insights into Sr_2RuO_4, which can be compared with the strain susceptibility measured by ultrasound. Two controversies that need to be resolved concerning the changes in T_c under strain are presented in detail in Box 2. One is the absence of a kink in the T_c versus strain, as anticipated from ultrasound. The other is the slope of the T_c versus strain curves for in-plane and out-of-plane compressional strains.

First, the absence of a kink in the variation of T_c with the [110] strain[22] is qualitatively incompatible with the observed jump in the ultrasound velocity of the shear mode c_{66} (refs. 30,31). The absence of a kink with the [100] strain is also not consistent with the μSR results, which suggests a two-component order parameter that contains a linear T_c increase and naturally leads to a kink. Watson et al. did not observe such a kink under compressional and tensile [100] strains[44]. Second, aside from the kink, the magnitude of the slopes of T_c versus strain with in-plane and out-of-plane compressional strains[22,41] is quantitatively different by a factor of about five from the observed ultrasound velocity jumps. Considering the precision of the strain and ultrasound experiments, these qualitative and quantitative disagreements pose a serious issue that requires attention.

In all these cases, the variations in T_c deduced from the ultrasound velocity jumps were substantially greater than those observed under the corresponding compressional strains. Concerning the difference in the magnitude of the ultrasound velocity jumps between the two groups[30,31], the role of the superconducting domains has been discussed[45]. We note that typical magnitudes of strain are as small as 10^{-4} in uniaxial strain experiments, 10^{-6} to 10^{-8} in pulse–echo ultrasound and 10^{-10} in resonant ultrasound spectroscopy. The difference in magnitude, in conjunction with the differences in the measurement frequency and configuration of the superconducting domains, may be crucial for resolving these controversies.

If the observed jump in c_{66} is reliable, this result provides strong evidence that the order parameter consists of two components. This is because the symmetry of the square of the order parameter contains the same representation as ε_6 (B_{2g}) to induce such a coupling. This is the case for $d_{yz} + d_{zx}$ (2D) and $d_{x^2-y^2} + g_{xy(x^2-y^2)}$ (accidentally degenerated). If such coupling with shear strain is absent, these candidate order parameters are unlikely.

Conclusion

We selected some promising candidates for the superconducting state of Sr_2RuO_4, as shown in Fig. 2. They are classified by the irreducible representations allowed in the point symmetry of D_{4h} applied to Sr_2RuO_4 without distortions. Except for the B_{1g} *d*-wave state, which is well known for high-T_c copper oxide superconductors, superconducting domains may form in a tetragonal lattice.

The E_g candidates are further divided into two types. One is the traditional unconventional pairing, for example, a chiral *d*-wave state with gap anisotropy $\Delta(\mathbf{k}) = \Delta_0 k_z(k_x + ik_y)$, and the other is the exotic interorbital pairing. The results of μSR support the TRS breaking 2D E_g candidates and two-component 1D order parameters. The results of shear ultrasound additionally support the TRS-preserving nematic E_g candidates. If the additional horizontal line node does not exist, the promising state is B_{1g} $d_{x^2-y^2}$ with a gap function $\Delta(\mathbf{k}) = \Delta_0(k_x^2 - k_y^2)$. In this case, the TRS is preserved, the second transition does not exist under uniaxial strain, the field angle-resolved specific heat needs reinterpretation and the superconducting domains do not form.

The 30-year history of the superconductivity of Sr_2RuO_4 has taught us how challenging it can be to thoroughly understand an unconventional superconductor. More than once, we have seen how an indispensable technique, although giving reproducible results among specialists, had to be revised. In this sense, Sr_2RuO_4 grew with the progress of modern-day condensed-matter physics. As in the comic, the community may still have to sacrifice some of the traditional knowhows to finally solve the Sr_2RuO_4 puzzle and fully open the gate of truth.

References

1. Bednorz, J. G. & Müller, K. A. Possible high T_c superconductivity in the Ba–La–Cu–O system. *Z. Phys. B* **64**, 189–193 (1986).
2. Maeno, Y. et al. Superconductivity in a layered perovskite without copper. *Nature* **372**, 532–534 (1994).
3. Mackenzie, A. et al. Extremely strong dependence of superconductivity on disorder in Sr_2RuO_4. *Phys. Rev. Lett.* **80**, 161–164 (1998).
4. Nakatsuji, S., Ikeda, S. & Maeno, Y. Ca_2RuO_4: New Mott insulators of layered ruthenate. *J. Phys. Soc. Jpn.* **66**, 1868–1871 (1997).
5. Maeno, Y., Yonezawa, S. & Ramires, A. Still mystery after all these years—unconventional superconductivity of Sr_2RuO_4. *J. Phys. Soc. Jpn.* **93**, 062001 (2024).
6. Mackenzie, A. P. & Maeno, Y. The superconductivity of Sr_2RuO_4 and the physics of spin-triplet pairing. *Rev. Mod. Phys.* **75**, 657–712 (2003).

7. Tamai, A. et al. High-resolution photoemission on Sr_2RuO_4 reveals correlation-enhanced effective spin–orbit coupling and dominantly local self-energies. *Phys. Rev. X* **9**, 021048 (2019).
8. Damascelli, A. et al. Fermi surface, surface states, and surface reconstruction in Sr_2RuO_4. *Phys. Rev. Lett.* **85**, 5194–5197 (2000).
9. Pustogow, A. et al. Constraints on the superconducting order parameter in Sr_2RuO_4 from oxygen-17 nuclear magnetic resonance. *Nature* **574**, 72–75 (2019).
10. Ishida, K., Manago, M., Kinjo, K. & Maeno, Y. Reduction of the ^{17}O Knight shift in the superconducting state and the heat-up effect by NMR pulses on Sr_2RuO_4. *J. Phys. Soc. Jpn.* **89**, 034712 (2020).
11. Chronister, A. et al. Evidence for even parity unconventional superconductivity in Sr_2RuO_4. *Proc. Natl Acad. Sci. USA* **118**, e2025313118 (2021).
12. Petsch, A. et al. Reduction of the spin susceptibility in the superconducting state of Sr_2RuO_4 observed by polarized neutron scattering. *Phys. Rev. Lett.* **125**, 217004 (2020).
13. Luke, G. et al. Time-reversal symmetry breaking superconductivity in Sr_2RuO_4. *Nature* **394**, 558–561 (1998).
14. Higemoto, W., Koda, A., Kadono, R., Yoshida, Y. & Onuki, Y. Investigation of spontaneous magnetic field in spin-triplet superconductor Sr_2RuO_4. *JPS Conf. Proc.* **2**, 010202 (2014).
15. Shiroka, T. et al. μSR studies of superconductivity in eutectically grown mixed ruthenates. *Phys. Rev. B* **85**, 134527 (2012).
16. Grinenko, V. et al. Split superconducting and time-reversal symmetry-breaking transitions in Sr_2RuO_4 under stress. *Nat. Phys.* **17**, 748–754 (2021).
17. Grinenko, V. et al. Unsplit superconducting and time reversal symmetry breaking transitions in Sr_2RuO_4 under hydrostatic pressure and disorder. *Nat. Commun.* **12**, 3920 (2021).
18. Xia, J., Maeno, Y., Beyerdorf, P. T., Fejer, M. M. & Kapitulnik, A. High resolution polar Kerr effect measurements of Sr_2RuO_4: evidence for broken time-reversal symmetry in the superconducting state. *Phys. Rev. Lett.* **97**, 167002 (2006).
19. Huddart, B. et al. Intrinsic nature of spontaneous magnetic fields in superconductors with time-reversal symmetry breaking. *Phys. Rev. Lett.* **127**, 237002 (2021).
20. Blundell, S. & Lancaster, T. DFT + μ: density functional theory for muon site determination. *Appl. Phys. Rev.* **10**, 021316 (2023).
21. Koyama, T. Comment on 'Charge expulsion and electric field in superconductors'. *Phys. Rev. B* **70**, 226503 (2004).
22. Hicks, C. W. et al. Strong increase of T_c of Sr_2RuO_4 under both tensile and compressive strain. *Science* **344**, 283–285 (2014).
23. Steppke, A. et al. Strong peak in T_c of Sr_2RuO_4 under uniaxial pressure. *Science* **355**, eaaf9398 (2017).
24. Maeno, Y. et al. Enhancement of superconductivity of Sr_2RuO_4 to 3 K by embedded metallic microdomains. *Phys. Rev. Lett.* **81**, 3765–3768 (1998).
25. Li, Y.-S. et al. High-sensitivity heat-capacity measurements on Sr_2RuO_4 under uniaxial pressure. *Proc. Natl Acad. Sci. USA* **118**, e2020492118 (2021).
26. Li, Y.-S. et al. Elastocaloric determination of the phase diagram of Sr_2RuO_4. *Nature* **607**, 276–280 (2022).
27. Beck, S., Hampel, A., Zingl, M., Timm, C. & Ramires, A. Effects of strain in multiorbital superconductors: the case of Sr_2RuO_4. *Phys. Rev. Res.* **4**, 023060 (2022).
28. Ghosh, S. K. et al. Recent progress on superconductors with time-reversal symmetry breaking. *J. Phys. Condens. Matter* **33**, 033001 (2020).
29. Fittipaldi, R. et al. Unveiling unconventional magnetism at the surface of Sr_2RuO_4. *Nat. Commun.* **12**, 5792 (2021).
30. Benhabib, S. et al. Ultrasound evidence for a two-component superconducting order parameter in Sr_2RuO_4. *Nat. Phys.* **17**, 194–198 (2021).
31. Ghosh, S. et al. Thermodynamic evidence for a two-component superconducting order parameter in Sr_2RuO_4. *Nat. Phys.* **17**, 199–204 (2021).
32. Anwar, M. S. & Robinson, J. W. A. A review of electronic transport in superconducting Sr_2RuO_4 junctions. *Coatings* **11**, 1110 (2021).
33. Deguchi, K., Mao, Z. & Maeno, Y. Determination of the superconducting gap structure in all bands of the spin-triplet superconductor Sr_2RuO_4. *J. Phys. Soc. Jpn.* **73**, 1313–1321 (2004).
34. Kittaka, S. et al. Searching for gap zeros in Sr_2RuO_4 via field-angle-dependent specific-heat measurement. *J. Phys. Soc. Jpn.* **87**, 093703 (2018).
35. Izawa, K. et al. Superconducting gap structure of spin-triplet superconductor Sr_2RuO_4 studied by thermal conductivity. *Phys. Rev. Lett.* **86**, 2653–2656 (2001).
36. Hassinger, E. et al. Vertical line nodes in the superconducting gap structure of Sr_2RuO_4. *Phys. Rev. X* **7**, 011032 (2017).
37. Khasanov, R. et al. In-plane magnetic penetration depth in Sr_2RuO_4: muon-spin rotation and relaxation study. *Phys. Rev. Lett.* **131**, 236001 (2023).
38. Mueller, E. et al. Superconducting penetration depth through a Van Hove singularity: Sr_2RuO_4 under uniaxial stress. *Phys. Rev. B* **110**, L100502 (2024).
39. Landaeta, J. et al. Evidence for vertical line nodes in Sr_2RuO_4 from nonlocal electrodynamics. *Phys. Rev. B* **110**, L100503 (2024).
40. Suh, H. G. et al. Stabilizing even-parity chiral superconductivity in Sr_2RuO_4. *Phys. Rev. Res.* **2**, 032023 (2020).
41. Jerzembeck, F. et al. The superconductivity of Sr_2RuO_4 under c-axis uniaxial stress. *Nat. Commun.* **13**, 4596 (2022).
42. Forsythe, D. et al. Evolution of fermi-liquid interactions in Sr_2RuO_4 under pressure. *Phys. Rev. Lett.* **89**, 166402 (2002).
43. Fukaya, Y., Hashimoto, T., Sato, M., Tanaka, Y. & Yada, K. Spin susceptibility for orbital-singlet Cooper pair in the three-dimensional Sr_2RuO_4 superconductor. *Phys. Rev. Res.* **4**, 013135 (2022).
44. Watson, C. A., Gibbs, A. S., Mackenzie, A. P., Hicks, C. W. & Moler, K. A. Micron-scale measurements of low anisotropic strain response of local Tc in Sr_2RuO_4. *Phys. Rev. B* **98**, 094521 (2018).
45. Ghosh, S. et al. Strong increase in ultrasound attenuation below T_c in Sr_2RuO_4: possible evidence for domains. *Phys. Rev. B* **106**, 024520 (2020).
46. Bobowski, J. et al. Improved single-crystal growth of Sr_2RuO_4. *Condens. Matter* **4**, 6 (2019).
47. Yonezawa, S. Bulk topological superconductors. *AAPPS Bull.* **26**, 3–11 (2016).
48. Bardeen, J., Cooper, L. N. & Schrieffer, J. R. Microscopic theory of superconductivity. *Phys. Rev.* **106**, 162–164 (1957).
49. Jerzembeck, F. et al. T_c and the elastocaloric effect of Sr_2RuO_4 under <110> uniaxial stress: no indications of transition splitting. *Phys. Rev. B* **110**, 064514 (2024).
50. Sigrist, M. Ehrenfest relations for ultrasound absorption in Sr_2RuO_4. *Prog. Theor. Phys.* **107**, 917–925 (2002).
51. Walker, M. B. & Contreras, P. Theory of elastic properties of Sr_2RuO_4 at the superconducting transition temperature. *Phys. Rev. B* **66**, 214508 (2002).

Acknowledgements

We thank A. P. Mackenzie, C. W. Hicks, S. Yonezawa, K. Ishida, A. Ramires, M. Sigrist, V. Grinenko, B. Ramshaw, J. Bobowski, M. Cuoco, T. A. Johnson, H. Matsuki and S. Paul for the critical reading of the article and useful information. In particular, information on the magnitudes of various strain experiments was provided by B. Ramshaw. The gap structure images shown in Fig. 2 were provided by S. Yonezawa. This study was supported by the Toyota Physical and Chemical Research

Institute (Toyota Riken). Y.M. acknowledges support from the JSPS KAKENHI No. JP22H01168. A.I. acknowledges support from JSPS KAKENHI No. JP24H01659. A.I. and G.M. acknowledge support from the Kyoto University Foundation. We also acknowledge the support of Dieter Schwarz Foundation for the QUASAR project.

Author contributions

Y.M. drafted the main part of the article, A.I. drafted Box 2 and G.M. devised and prepared most of the artwork. All authors contributed to discussing the content, editing and revising the article.

Competing interests

The authors declare no competing interests.

Additional information

Correspondence should be addressed to Y. Maeno.

Peer review information *Nature Physics* thanks Stephen Blundell and Zhiqiang Mao for their contribution to the peer review of this work.